Langmuir

Article

pubs.acs.org/Langmuir

A Nonenzymatic Biosensor Based on Gold Electrodes Modified with Peptide Self-Assemblies for Detecting Ammonia and Urea Oxidation

Roberta C. Bianchi,[†] Emerson Rodrigo da Silva,[†] Luiz H. Dall'Antonia,[‡] Fabio Furlan Ferreira,[†] and Wendel Andrade Alves*[,†]

[†]Centro de Ciências Naturais e Humanas, Universidade Federal do ABC, 09210-580 Santo André, SP Brazil

[‡]Departamento de Química, Centro de Ciências Exatas, Universidade Estadual de Londrina, 86057-970 Londrina, PR Brazil

Supporting Information

ABSTRACT: We have developed a nonenzymatic biosensor for the detection of ammonia and urea oxidation based on the deposition of peptide microstructures onto thiolated gold electrodes. FF-MNSs/MCP/Au assemblies were obtained by modifying gold substrates with 4-mercaptopyridine (MCP), followed by coating with L,L-diphenylalanine micro/nanostructures (FF-MNSs) grown in the solid-vapor phase. Benzene rings and amide groups with peptide micro/nanostructures interact with synthetic NH_4^+ receptors through cation−π and hydrogen bonding. AuOH clusters on the Au surface provided the catalytic sites. The application of a predetermined concentration of analytes at the peptide interfaces activated the catalytic sites. We observed a relationship between the stability of films and the crystal structure of peptides, and we organized the FF-MNSs into an orthorhombic symmetry that was the most suitable assembly for creation of our biosensors. At 0.1 mol L^{-1} NaOH, these FF-MNSs/MCP/Au electrodes have electrocatalytic properties regarding ammonia and urea oxidation that are comparable to those of enzyme-based architectures. Under optimal conditions, the electrocatalytic response is proportional to the ammonia and urea concentration in the range 0.1−1.0 mmol L^{-1}. The sensitivity was calculated as 2.83 and 81.3 μA mmol L^{-1} cm^{-2} for ammonia and urea, respectively, at +0.40 V (vs SCE). Our detection method is easy to follow, does not require a mediator or enzyme, and has strong potential for detecting urea via nonenzymatic routes.

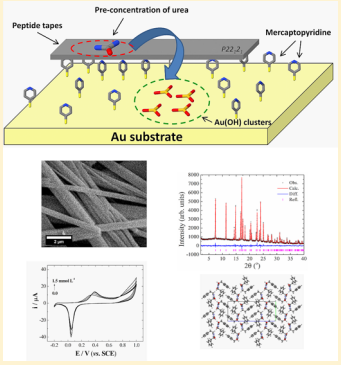

1. INTRODUCTION

Urea is widely observed in nature, and its analysis is of considerable interest in many fields, including clinical and agricultural chemistry.[1] It plays a paramount role in the metabolism of mammals and is recognized as an important marker for evaluating uremic toxin levels.[2] For example, the normal level of urea in human serum ranges from 2.5 to 7.5 mmol L^{-1}. In patients suffering from renal insufficiency, this concentration may be as high as 30−80 mmol L^{-1}, concentrations at which hemodialysis is required.[3] Therefore, the appropriate detection of urea at biologically relevant conditions is of utmost importance. An ideal sensor should exhibit numerous nontrivial characteristics, such as biocompatibility, high sensitivity, accuracy, selectivity, and a low cost of production.

In recent years, several methods have been exploited for urea detection, including liquid chromatography, isotopic-dilution mass spectrometry, chemiluminescence, and devices based on potentiometry and amperometry.[4,5] However, the complexity of fabrication is often a major drawback to these approaches.[6] Electrocatalytic oxidation of urea in an alkaline medium has been investigated using different metal electrodes, especially platinum (Pt), which produces NH_4^+ ions at potentials from 0.06 to 0.3 V.[7] Nevertheless, Pt-based systems are very nonselective and are susceptible to poisoning upon long-term contact with physiological fluids.[8] In this context, gold substrates are attractive for urea sensing because their oxidation potential at neutral and alkaline pHs is more negative compared to those of other metals.[9] Furthermore, the ease of functionalization and biological inertness makes gold an interesting support for biosensing devices.

Peptides can form hybrid compounds with many metallic species, including gold. Previous studies have attempted to control the self-assembly of peptide-based structures, mainly because of their applicability in biotechnological systems such as molecular carriers, optoelectronic devices, and biological sensors.[10] Among several sequences that can form self-ordered materials, the homo dipeptide L,L-diphenylalanine (FF) has been extensively investigated. Specifically, several studies have reported 1D morphologies, usually rodlike in shape, with a high aspect ratio and diameters ranging from tens of nanometers up to a few micrometers.[11,12] However, the crystallographic arrangement has been described by the hexagonal space group $P6_1$ when self-assembly occurred in a water-rich medium.[13] In this symmetry, linear FF units self-assemble into cyclic hexamers via H-bonds mediated by H_2O molecules. According to this multiscaled framework, the carboxyl and amine groups turn inward toward the peptide matrix, whereas

Received: June 16, 2014
Revised: August 5, 2014
Published: September 4, 2014

benzene rings remain at the outer interfaces, making the interfaces highly hydrophobic. In addition, $\pi-\pi$ interactions occur, and hexamers stack into columnar phases, thereby leading to narrow hydrophilic tunnels able to host polar species.[14] In contrast, the molecular organization of the FF units is composed of orthorhombic groups when self-assembly occurs under anhydrous conditions.[15] Lee et al. have suggested that, in the absence of water to stabilize the linear form, carboxyl and amine groups at the dipeptide backbone fuse together (3,6-bis(phenylmethyl)-2,5-piperazinedione), forming cyclo-FF.[16] This structure is compact, with no internal empty space.

Over the past decade, studies have investigated the capabilities of FF self-assemblies for biosensing purposes. In their early research, Yemini et al. reported the production of L,L-diphenylalanine micro/nanostructures (henceforth, FF-MNSs) in solution, followed by deposition onto graphite electrodes.[17] Their results showed significant improvements in the sensitivity for the electrochemical reactivity of potassium hexacyanoferrate redox, and the assembly effectively detected H_2O_2 using peroxidase and 4-acetaminophenol as mediators. In a similar study, thiol-modified FF-MNSs were applied onto gold substrates, and the resulting electrode exhibited a high sensitivity for monitoring H_2O_2 produced by enzymatic reactions of glucose and glucose oxidase.[18] Recently, our group developed a hybrid architecture by combining FF-MNSs and polymer electrolyte membranes for the detection of dopamine.[19] Glassy carbon + Nafion electrodes were coated with FF-MNSs, and cyclic-tetramer copper(II) species containing the ligand (4-imidazolyl)-ethylene-2-amino-1-ethyl-pyridine $[Cu_4(apyhist)_4]^{4+}$ were used to mediate catalysis. In another approach, a biosensor was fabricated using micro-peroxidase-11 (MP11) as an electrocatalyst combined to FF-MNSs as a supporting matrix. The resulting hybrid led to an effective bioelectrochemical interface for the detection of H_2O_2 with ITO electrodes. The FF-MNSs provided a favorable microenvironment for the MP11-mediated direct electron transfer to the electrode surface.[20]

Notably, a common feature shared by the aforementioned sensing architectures is the need to functionalize FF-MNSs with mediators for catalyzed redox reactions. As a rule, biosensors aimed at urea detection also require a mediated, often enzymatic, route to perform electrocatalysis. Here, we define a novel alternative scheme for preparing an enzyme-free system that detects urea through a combination of peptide assemblies and thiolated gold substrates. FF-MNSs were deposited onto thiol-modified surfaces, providing a unique bioinspired architecture with a large interfacial area, numerous benzene rings and AuOH catalyst sites. We hypothesize that this assembly creates receptors via intense H-bonding or cation$-\pi$ interactions between NH_4^+ species and aromatic groups available at the peptide interface. AuOH clusters form directly onto Au substrates and provide the necessary catalyst sites for redox reactions. Previous theoretical studies[21] have suggested that cation$-\pi$ interactions and H-bonding between substrates and central benzene rings play a significant role in determining the binding affinity and provide a partial selectivity toward NH_4^+ receptors. In this context, our peptide-modified electrodes have potential as a biosensing platform for the molecular recognition of ammonium ions and urea in solution, making them good candidates for new ionophores[22] or peptide mimicry.[23] In addition, the electrodes presented here provide nonmediated electron transfer, a short detection time, a high current density, and high stability.

2. EXPERIMENTAL SECTION

2.1. Materials. All reagents used were of analytical grade. Ammonium and sodium hydroxides, sulfuric acid, absolute ethanol, and methanol were purchased from Synth (Brazil). Aniline, 4-mercaptopyridine (MCP), L,L-diphenylalanine, and 1,1,1,3,3,3-hexafluoro-2-propanol (HFIP) were obtained from Sigma-Aldrich. With the exception of aniline, which was distilled prior to use, all reagents were used as received. All solutions were prepared using ultrapure water from a Milli-Q system (resistivity > 18 MΩ cm^{-1}).

2.2. Preparation of FF-MNSs onto a Gold Electrode Surface (FF-MNSs/MCP/Au). We began the preparation of our biosensors by polishing gold electrodes (geometrical surface area = 0.07 cm^2) with alumina. After this first abrasive cleaning, the electrodes were subjected to approximately 80 potential cycles from −0.2 to 1.6 V (vs SCE) at a scan rate of 0.5 mV s^{-1} in a 0.5 mol L^{-1} H_2SO_4 solution. Next, the substrates were dropped into 100 mmol L^{-1} MCP solutions for 2 h to coat the metallic surface with a thiol layer. The self-assembly of FF-MNSs was performed directly on the substrates using a variation of the solid-vapor-phase approach proposed by Ryu and Park.[24] This method was also detailed in a previous work.[25] Briefly, we dissolved FF in HFIP to a concentration of 100 mg mL^{-1} and cast an aliquot from this solution onto the MCP layer to form an amorphous peptide film. Next, samples were incubated within a chamber saturated with water vapor or aniline vapor for 12 h at 98 °C and at normal pressure. After this procedure, the FF-MNSs/MCP/Au electrodes were ready for use in electrochemical studies. To avoid aggregation and aging problems, fresh peptide solutions were prepared immediately prior to use. Photographs exhibiting the final aspect of our electrodes are shown in Supporting Information Figure S1.

2.3. X-ray Diffraction and Electron Microscopy. X-ray diffraction (XRD) patterns of powdered samples were recorded at room temperature on a Stadi-P (Stoe, Darmstadt, Germany) diffractometer (transmission configuration). The beam was provided by a Cu-target source and produced monochromatic X-ray photons of λ = 0.154056 nm; the source was operated at 40 kV and 40 mA. The samples were scraped from the electrodes and crumbled to obtain a fine powder. Next, the samples were sandwiched between acetate-cellulose foils (Ultraphan) and rotated during acquisition. A Mythen 1K silicon strip detector was used for data collection. The 2θ range was scanned between 2° and 40°. Scanning electron microscopy (SEM) images were obtained using a JEOL LV-SEM microscope operated at a voltage of 15 kV at the LME/LNNano (Laboratory of Electron Microscopy of the Nanotechnology National Laboratory, Campinas, Brazil). The beam accelerating voltage ranged between 5 and 25 kV, and samples were coated with a thin Pt layer prior to imaging.

2.4. Electrochemical Measurements. Cyclic and square-wave voltammetry (CV and SWV, respectively) were performed using a μAutolab Fra 2, Type III potentiostat/galvanostat. pH measurements were obtained with a Metrohm-Pensalab 827 pH meter equipped with combined glass electrodes. All electrochemical measurements were performed in a conventional three-electrode electrochemical cell. The FF-MNSs/MCP/Au assembly was the working electrode, Pt wire was used as the auxiliary electrode, and a saturated calomel electrode (SCE) was used as a reference electrode. CV experiments were performed by applying a potential between −0.2 to 1.0 V vs SCE at scan rate of 25 mV s^{-1}. Square-wave voltammetry (SWV) assays were completed by applying a frequency of 50 Hz, a pulse amplitude of 70 mV, and step potential of 2 mV vs SCE. The supporting electrolyte was a solution of 0.1 mol L^{-1} NaOH.

3. RESULTS AND DISCUSSION

3.1. Morphology and Structure. Morphology and structure play a key role in the behavior of the sensing devices described here. For example, small variations in the shape and size of self-assemblies cast onto electrodes strongly affect the

dx.doi.org/10.1021/la502315m | Langmuir 2014, 30, 11464−11473

surface area and have direct consequences on catalytic properties. However, the spatial organization of peptides at a molecular level has been shown to closely relate to electronic properties.[26,27] We have previously reported that a crystalline symmetry drives the hydrophobicity of the peptide interface for FF-based assemblies.[15] Our samples were prepared using water or aniline vapor. These solvents exhibit very distinct chemical properties and are known to form different crystallographic symmetries in the resulting assemblies.[15,16,25]

To determine these characteristics in our thiol-modified electrodes, we performed a thorough analysis using SEM. In Figure 1, scanning electron micrographs from samples obtained

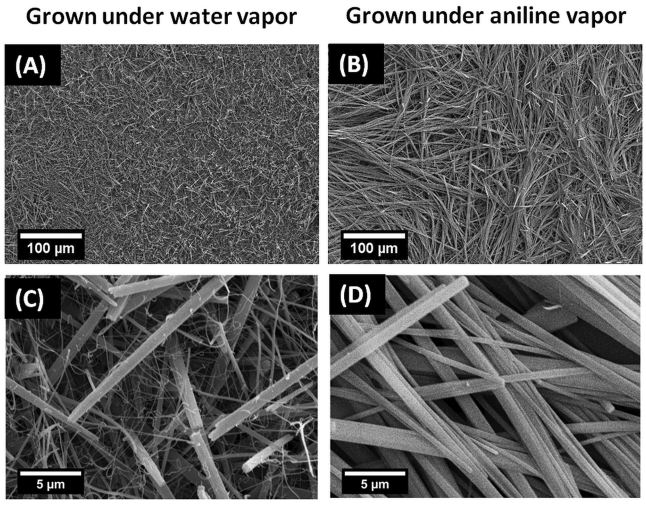

Figure 1. Scanning electron micrographs of FF-MNSs/MCP/Au electrodes at different magnifications. Images on the left side (A and C) correspond to structures self-assembled under water vapor, whereas those on the right side (B and D) were obtained using aniline in the gas phase.

either under water vapor or under aniline vapor are shown. For both solvents, we observed elongated polymorphs homogeneously spread across the surface and an intricate network covering the electrodes (Figure 1A and 1B). Important differences in the size of the arrays between the two solvents were observed. Structures obtained under water vapor had lengths that averaged between 20 and 30 μm, whereas aniline-incubated assemblies were much larger, with a subset reaching greater than 100 μm. Figure 1C and 1D shows high-magnification images of the samples that highlight their novel morphological features. In contrast to previous studies that reported that the solid-vapor approach led to rodlike structures,[16,24,25] we observed flat micrometric tapes. This finding is a very unique aspect of our system because the flat surface of tapes can facilitate the buildup of analytes onto electrodes. Estimation of the tapes from different micrographs (N = 100) revealed that the average thicknesses were 1.9 ± 0.4 and 2.8 ± 0.8 μm for the structures grown under water and aniline vapor, respectively. In addition, samples obtained under water vapor (Figure 1A and 1C) exhibited the coexistence between nanosized rodlike filaments and micrometric flat tapes. We believe that these fibers are intermediate residues of an incomplete assembly process because water-grown arrays are smaller than aniline-incubated structures in length and thickness; that is, aniline vapor leads to higher self-assembly efficiency and implies larger and homogeneous tapes. Moreover, the presence of 4-mercaptopyridine likely plays a relevant role, presumably via $\pi-\pi$ interactions between pyridine and benzene rings[28] (see discussion on next section), regarding appearance of flat morphologies. In this case, the availability of heteroatoms at pyridine rings could enable stronger interfacial interactions between peptides and substrate favoring self-assembly into flat tapes.[29] Moreover, as aforementioned, in other contexts, where structures have been grown directly onto the substrate, aniline vapor has led to rodlike structures (e.g., nanowires).[16,24,25]

To characterize our structures at the crystallographic level, we performed powder diffraction experiments. Figures 2 and 3 show high-resolution XRD patterns of both water- and aniline-incubated samples. For arrays obtained using H_2O in the gas phase, the diffraction pattern is indexed to the hexagonal ($P6_1$) space group, as previously described by Gorbitz.[13] To accurately determine the crystal structure, we used the structural model devised by Gorbitz to generate Rietveld refinements.[30] Despite the symmetry of this structural model leading to correct predictions of peak positions in our diffraction patterns, a lack of agreement of some reflections and deviations at predicted intensities were evident (data not shown). The fit did not improve after the water molecules were removed from the diphenylalanine unit cell. For the Rietveld refinement, the background was fitted using a 12-term Chebyshev polynomial. The peak asymmetry was adjusted using the simple axial divergence model of Cheary and Coelho.[31] The peak profiles were modeled using the fundamental parameters approach[32] with a fourth-order spherical harmonics[33] function to correct for the preferred orientation of the crystallites. The isotropic atomic displacements (B_{iso}) were constrained to be equal for all non-hydrogen atoms. For the hydrogen atoms, the B_{iso} values were constrained to be 1.2 times larger than the values of the respective atoms to which they were connected. The structural coordinates were not refined. Only the unit cell parameters were allowed to vary. The major differences that likely accounted for misfit intensities were attributed to the number and geometrical arrangement of water molecules within the unit cell. In this context, as an alternative to the Gorbitz model, we have introduced guest water molecules into the hydrophilic channels of the peptide matrix. The average number of H_2O molecules per hexamer in $P6_1$ FF assemblies was determined to be between 15 and 24.[34,35] Moreover, in a recent theoretical study, water molecules were observed to strongly bind to FF nanotubes, with the strongest interaction appearing when the matrix hosts 17 H_2O molecules per hexamer.[26] On the basis of these data, we included the corresponding number of water molecules in the channels of the diphenylalanine matrix, which formed on the corners of the unit cell and are represented along the c-axis. Although the fractional coordinates of the diphenylalanine unit cell were not refined, the H_2O molecules (three of them were inserted) and their occupancy within the unit cell were varied. The hydrogen atoms of the water molecules were geometrically inserted using the Mercury software program.[36] Under these conditions, the true orientation of the hydrogen atoms may differ from what was represented. As expected, the sum of partial occupancies of the three water molecules resulted in unity within the asymmetric unit. Because the number of formula units per unit cell was Z = 6, the total number of water molecules within the unit cell was 24. The final refined values for the unit-cell parameters after the Rietveld fit are shown in Figure 3. These values were a =

dx.doi.org/10.1021/la502315m | Langmuir 2014, 30, 11464−11473

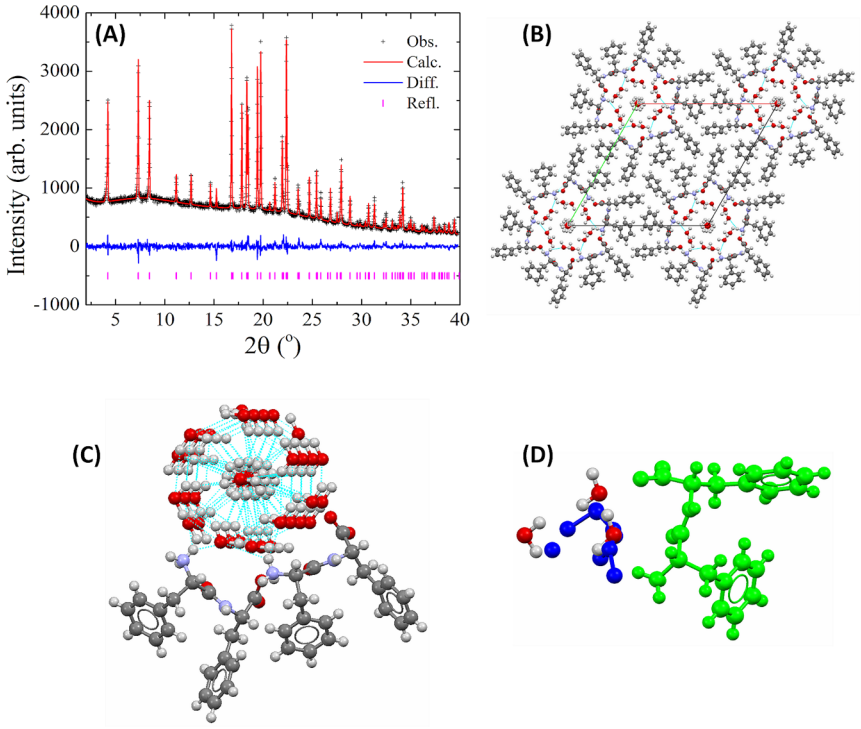

Figure 2. XRD assays of FF-MNSs obtained under water vapor. (A) Experimental data (black crosses) and the corresponding Rietveld refinement (red line). The blue line displays the difference between observed and calculated data, whereas the magenta bars at the bottom of the graph indicate the Bragg reflections of the hexagonal ($P6_1$) phase. (B) The $P6_1$ space group is represented along the *c*-axis. The phase hosts H_2O molecules in the core of FF rings that appear connected by the solid lines delimiting the unit cell. (C) A detailed view of the structure showing water molecules arranged along the *c*-axis, where the water molecules form an infinite chain organized into a helixlike conformation. (D) Schematic drawing of water molecules arranged into the asymmetric unit of the structure determined by Gorbitz[13] (blue) and the structure presented herein (red/white).

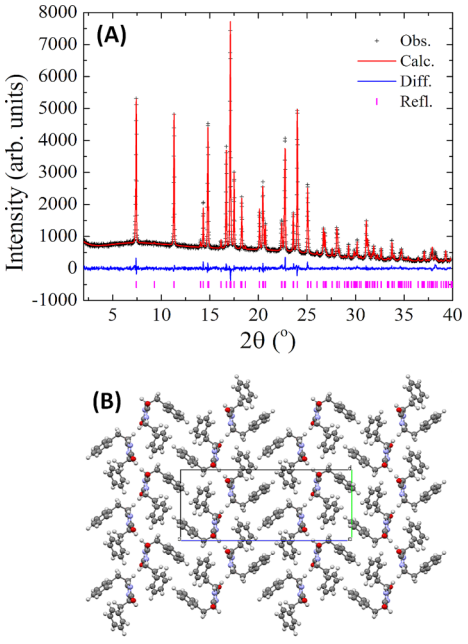

Figure 3. XRD assays from FF-MNTs obtained under aniline vapor. (A) Powder diffraction data (black crosses) with the corresponding Rietveld plot (red line) are shown. The blue line shows the differences between experimental and calculated data, and the magenta bars indicate the Bragg reflections predicted on the basis of an orthorhombic $P22_12_1$ phase. (B) Crystal structure packing obtained from our refinements. The solid lines delimit the $P22_12_1$ unit cell.

24.1616(10) Å, c = 5.4485(2) Å, V = 2754.62(26) Å^3, and ρ_{calc} = 1.1950 g cm^{-3}. The goodness-of-fit indicators and *R*-factors,[37] R_{Bragg}, R_{wp}, and R_{exp}, were χ^2 = 1.244, R_{Bragg} = 2.712%, R_{wp} = 4.875%, and R_{exp} = 3.917%. The weighted Durbin–Watson statistic (d-DW = 0.89) was quite low, indicating that the standard deviations are underestimated. No adequate physical model exists for correcting the standard deviation values in the Rietveld method to make them representative of repeated experiments.

Figure 2B shows the crystal packing of our FF structures treated with water vapor; the packing is shown along the *c*-axis and is displayed with a portion of the hydrogen interactions (cyan dashed lines). A fraction of the water molecules interacted with the diphenylalanine via hydrogen bonding. Interestingly, other water molecules were arranged along the *c*-axis, thus forming an infinite chain in a helixlike conformation (Figure 2C). This finding suggests that these hexagonally organized FF structures can function as proton-conducting channels and that these structures may have applications in ionic-transporter membranes. Our findings provide insight into the crystal structure of FF-MNSs obtained under a water-vapor route and figure out that the alternative to the Gorbitz model[13] devised here may be more accurate to describe these systems. Figure 2D highlights the differences between the arrangements of water molecules in the asymmetric unit of the structure determined by Gorbitz and the one we present here. These differences are responsible for the misfit of some of the intensities in the Rietveld refinement.

The diffraction peaks for FF-MNTs treated with aniline vapor, as shown in Figure 3A, are clearly different, suggesting a different crystal structure. This new phase was indexed to an

dx.doi.org/10.1021/la502315m | *Langmuir* 2014, 30, 11464–11473

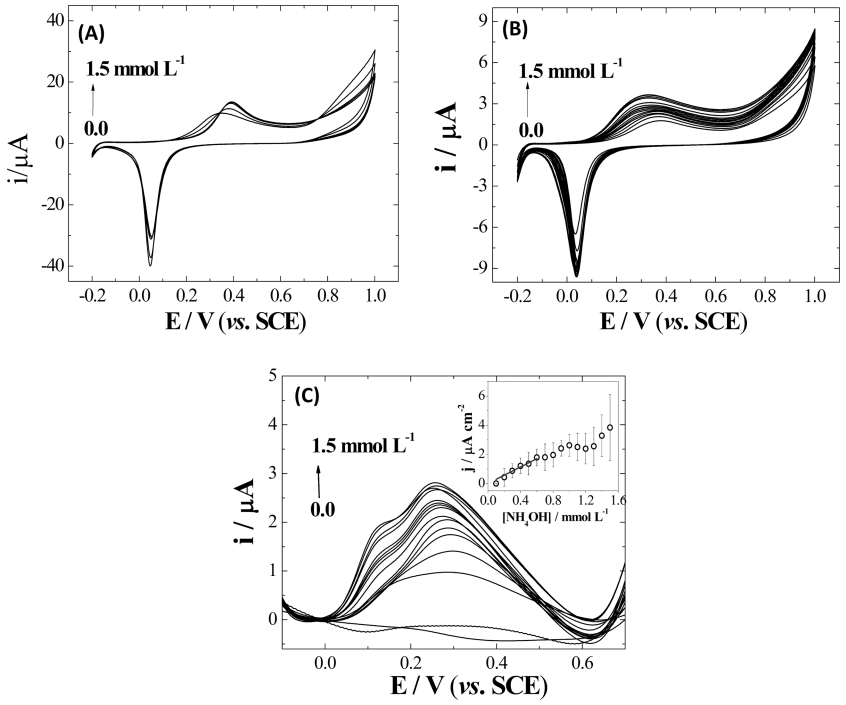

Figure 4. Cyclic voltammograms for FF-MNSs/MCP/Au electrodes synthesized under (A) water vapor and (B) aniline vapor with NH_4OH addition. The assays were conducted with a scan rate = 25 mV s^{-1} after the addition of NH_4OH at concentrations ranging from 0.0 to 1.5 mmol L^{-1}. (C) Square-wave voltammetry with the addition of ammonia (0.1−1.5 mmol L^{-1}) is shown for the following conditions: frequency = 50 Hz, amplitude = 70 mV, and ΔE_s = 2 mV. Electrolyte: NaOH at 0.1 mol L^{-1}, pH = 9. The inset shows the analytical curves obtained at +0.3 V.

orthorhombic crystal system with space group $P22_12_1$, as first proposed by Gdaniec and Liberek[38] and recently used to describe FF microtubes that self-assembled into aqueous solutions and had undergone thermally induced phase transition.[15] Figure 3A shows the results of the Rietveld refinement, and more details on the fitting procedure can be found elsewhere.[15] A good visual fit, good statistical *R*-factors, and satisfactory goodness-of-fit indicators were obtained. The refined unit cell parameters and statistical factors were a = 6.1764(3) Å, b = 10.3637(4) Å, c = 23.7851(10) Å, V = 1522.5(1) Å^3, χ^2 = 1.109, R_{Bragg} = 1.655%, R_{wp} = 4.215%, and R_{exp} = 3.800%. The crystal structure packing of FF-MNTs treated with aniline vapor is shown in Figure 3B.

3.2. Electrochemical Catalysis of the FF-MNSs/MCP/Au Electrode in Ammonia and Urea Oxidation. Before using our electrodes for urea sensing, we carried out cyclic voltammetric (CV) assays to elucidate the redox behavior of the electrodes in the presence of ammonium ions in solution. Urea is well-known to undergo hydrolysis by urease in aqueous solutions based on the following the equation:[8] $(NH_2)_2CO + 3H_2O \rightarrow CO_2 + 2NH_4OH$. In addition, ammonium ions were obtained in contact with Pt electrodes in the potential range 0.06−0.3 V (vs saturated hydrogen electrode, SHE), and its formation was confirmed using Nessler's solution. Thus, ammonium ions are an important intermediate appearing in the catalysis of urea, and its detection by our system represents a step toward the goal of detecting urea.

In Figure 4A, we show the voltammograms obtained from electrodes containing FF-MNSs organized into the hexagonal phase. When aliquots of NH_4OH were added to the electrolyte solution at concentration intervals between 0.1 and 1.5 mmol L^{-1}, we observed a clear anodic peak at E_{pa} = +0.4 V, accompanied by its cathodic counterpart at E_{pc} = +0.04 V. Both peaks can be attributed to the oxidation and reduction of gold oxyhydroxide (AuO or $Au(OH)_2$) species formed on the surface of the electrode.[9] Despite this remarkable initial catalytic behavior, we determined that the system does not remain stable. It eventually exhibits low adhesion of the particles to the substrate and presents a loss of peptide assemblies, followed by a strong decrease of the electrochemical response after a few potential cycles. The release of material is corroborated by a shift on the oxidation potential in Figure 4A, where a clear isosbestic point appears at +0.34 V. This crossover point is likely related to leaching of peptides from the electrode surface, resulting variation of potential of the electric double layer. We have ascribed this electrochemical leaching to the unique behavior of interactions between pyridine units at mercaptopyridine layer and benzenes at peptide assemblies. Pyridine rings are able to interact among themselves and with aromatic groups through strong $\pi-\pi$ stacking interactions.[28] Since in the solid-vapor method mercaptopyridine molecules are previously anchored at the substrate via Au−S interactions, their pyridine units are not free to turn or intercalate in the peptide matrix to establish $\pi-\pi$ interactions with benzene rings. As shown in Figure 2B, $P6_1$ symmetry exhibits aromatic hexamers forming a highly packed columnar phase, oriented parallel to the long axis of the assembly. In this configuration, steric hindrances presumably prevent the formation of $\pi-\pi$ bonds with pyridine trapped into thiol layer, making interactions between FF-MNSs and substrate weaker. Furthermore, the outer surface of FF-MNSs is very hydrophobic in the hexagonal phase,[15,39,40] which contributes to the weakening of interactions with mercaptopyridine (hydrophilic).

CV plots from electrodes obtained under aniline vapor are shown in Figure 4B. Unlike electrodes organized into $P6_1$ symmetry, these electrodes appear to be very stable in that they continue to exhibit electrocatalytic behavior after several voltammetric cycles. This stability results from the singular

dx.doi.org/10.1021/la502315m | *Langmuir* 2014, 30, 11464−11473

Table 1. Performance Comparison of Ammonium-Ion Sensors Based on Different Electrode Materials[a]

electrode	sensitivity (μA mmol^{-1} L cm^{-2})	linear range (mmol L^{-1})	LOD (μmol L^{-1})	ref
PPy nanowires/Au	6.15	not specified	4.8	47
PANI-PSSMA(II)/Au/Al_2O_3	10.5	0−12	not specified	48
PANI-Nafion/Pt−C	40 ± 20	0.005−1	5.0	49
L-glutamic acid hydrochloride/SAW devices	not specified	0−0.56	30	50
Porous SiC/*p*-type Si wafer/Al	not specified	0−0.56	27	51
FF-MNSs/MCP/Au	2.83	0.1−1	170	present work

[a]PPy, polypyrrole; PANI, polyaniline; PSSMA(II), poly(styrenesulfonate-*co*-maleic acid, sodium form); SAW, surface acoustic wave delay lines.

structural aspects of the FF-MNSs, now organized into an orthorhombic symmetry. In this organization, the columnar phases observed in the $P6_1$ arrangement are no longer found and benzene rings lying at the outer surface of the assemblies are able to form T-shaped $\pi-\pi$ stacking with pyridine rings. Furthermore, nitrogen and oxygen sites provide a mixed hydrophobic/hydrophilic interface with higher affinity toward pyridine and enable H-bonding interactions. Here, the tapes can establish stronger interactions with pyridine rings at the thiolated layer. This finding is a remarkable example of the key role of the crystal structure in sensing architectures and highlights the unique features provided by utilization of aniline in the gas phase during incubation. Similar to the first electrode, this system exhibited an anodic peak E_{pa} at approximately +0.4 V and a cathodic maximum at $E_{pc} \approx +0.05$ V (vs SCE) because of the redox reactions of gold oxyhydroxide (AuO or $Au(OH)_2$) species on the substrate.[9] However, the modified electrode exhibited a decreasing potential, together with an increasing anodic peak current, upon addition of NH_4OH, indicating catalytic activity toward ammonia oxidation. All measurements were performed in triplicate, and the results are indicated as the mean value. Moreover, the bare gold electrode showed negligible activity in an alkaline medium containing an ammonia solution (data not shown). These findings suggest that the FF-MNSs preconcentrate NH_4^+ ions and facilitate redox reactions in gold oxide clusters at the substrate. Indeed, gold functions as an active electrocatalyst in alkaline media by adsorbing hydroxyl groups to facilitate oxidation reactions.[9,41,42] However, ammonia does not exhibit a strong interaction at the gold surface because it does not adsorb or is weakly adsorbed and is restricted to a specific orientation of gold.[9,41,43] Our FF-MNSs/MCP/Au electrodes exhibited improved catalytic performance in this medium, most likely because of the formation of inclusion complexes between the FF-MNSs and NH_4^+ ions on the electrode surface; these complexes thus facilitated electronic transfer from one component to its counterpart.

Concentration studies were performed by investigating the response of the FF-MNSs/MCP/Au electrode to different concentrations of NH_4OH (Figure 4C) using SWV, which is a common electroanalytical technique used in quantitative analysis because of its sensitivity. At NH_4^+ ion concentrations greater than 0.6 mmol L^{-1}, the current did not further increase; this phenomenon is typically attributed to the saturation of catalytic sites. A linear relationship (eq 1) was observed between the current response and the concentration (inset in Figure 4C) in the concentration range from 0.1 to 1.0 mmol L^{-1}:

$$I_p\ (\mu A) = (2.83 \pm 0.16)\ [NH_4^+]/\text{mmol L}^{-1} \quad (1)$$

The sensitivity was calculated as 2.83 μA cm^{-2} mmol^{-1} L, whereas the limit of detection (LOD) was determined to be 0.17 mmol L^{-1}. These values are comparable with those previously reported in the literature. Specifically, our LOD was significantly lower, and the sensitivity was comparable to that of other electrodes modified with nanoparticles for ammonia detection (see Table 1).

The electroanalytical performance of the FF-MNSs/MCP/Au electrodes with respect to urea detection was investigated under the previously described working conditions. The cyclic and square-wave voltammograms from these assays are shown in Figure 5. The oxidation of urea in an alkaline medium was

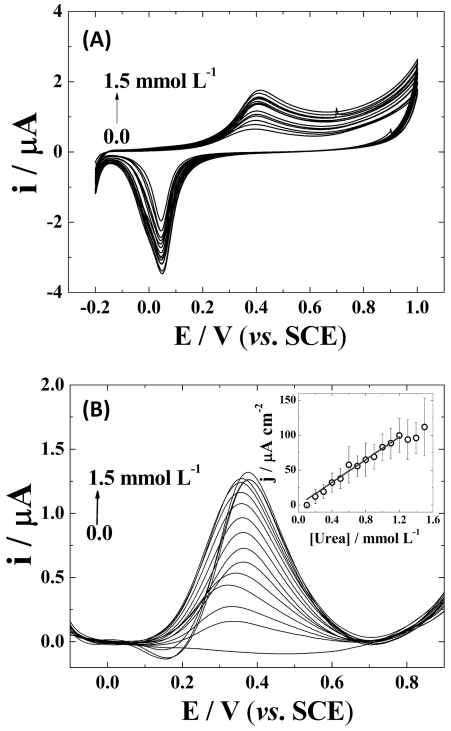

Figure 5. (A) Cyclic voltammograms from FF-MNSs/MCP/Au electrodes synthesized underaniline vapor after the addition of urea at concentrations ranging from 0.1 to 1.5 mmol L^{-1}. Electrolyte: NaOH 0.1 mol L^{-1} and scan rate = 25 mV s^{-1}. (B) Square-wave voltammetry with the addition of urea (0.1−1.5 mmol L^{-1}). Frequency = 50 Hz, amplitude = 70 mV, and ΔE_s = 2 mV. Electrolyte: NaOH 0.1 mol L^{-1}. The inset represents the analytical curves obtained at +0.4 V.

observed to occur at potentials greater than +0.35 V,[44] as shown in Figure 5A. The analytical curve shown in Figure 5B (inset) indicates a linear response in the concentration range of 0.1−1.1 mmol L^{-1}, in accordance with eq 2:

$$I_p\ (\mu A) = (81.27 \pm 1.75)\ [\text{urea}]/\text{mmol L}^{-1} \quad (2)$$

The current sensitivity and LOD were determined as 81.27 μA cm^{-2} mol^{-1} L and 0.06 mmol L^{-1}, respectively.

dx.doi.org/10.1021/la502315m | Langmuir 2014, 30, 11464−11473

Table 2. Comparison of Other Urea Sensors Described in the Literature[a]

bioelectrode	sensitivity (μA mmol L^{-1} cm^{-2})	linear range (mmol L^{-1})	LOD (mmol L^{-1})	ref
Urs-GLDH/MLG/ITO	32	1.66−16.6	0.6474	52
Urs-GLDH/ZnO-Ch/ITO	0.13	0.8−16.6	0.49	53
Urs/PAPCP/ITO	0.47	0.16−5.02	0.020	54
Urs-PANI-Nafion/Au	4.2	1−10	1	55
Urs-SWCNTs/glassy carbon	not specified	0.1−1 (nonlinear)	0.1	56
MWCNTs/silica	2.3	2.18×10^{-2}−1.07	not specified	57
Urs-Poly(5-NH_2-1-NAP)/PPy/Pt	0.58−3.44	up to 100	0.22−0.58	58
FF-MNSs/MCP/Au	81.3	0.1−1.0	0.060	present work

[a]Urs, urease; GLDH, glutamate dehydrogenase; MLG, multilayer graphene; ITO, indium tin oxide; PAPCP, poly(aminopropyl pyrrole-*co*-pyrrole); PANI, polyaniline; MWCNTs, multiwalled carbon nanotubes; SWCNTs, single-walled carbon nanotubes; poly(5-NH_2-1-NAP), poly(5-amino-1-naphthol); PPy, polypyrrole.

A comparison of the sensing characteristics of our FF-MNSs/MCP/Au electrodes with previous studies is shown in Table 2. We observe that the modified gold electrodes exhibited enhanced sensitivity toward urea detection, despite their simple preparation protocol and the lack of enzyme mediators. Notably, the cooperative effect of nanostructured materials significantly increased the sensitivity of the electrode.

AuOH species on the electrode surface likely played a key role in the mechanism of urea hydrolysis. The main evidence to support this statement is the redox signature of Au oxides,[9] and their characteristic anodic/catodic peaks at E_{pa} = +0.4 V and E_{pc} = +0.04 V, which is clearly observable even for electrodes coated with mercaptopyridine (see Figure 4 and Supporting Information Figure S2). The surface coverage by Au oxide or thiol coating (assumed to be a monolayer) can be estimated from the simple equation $\Gamma = Q/nFA$, where Γ is the number of molecules per area, Q is the charge transferred in the redox reaction, n is the number of electrons per molecule involved in the reaction (herein n = 1 either for thiol or for Au redox), F is the Faraday constant (=96 500 C mol^{-1}), and A is the geometrical area of the electrode (=0.07 cm^2). From voltammetric data (Supporting Information, Figure S2), we have determined Q by integrating anodic peaks of both Au oxide and thiol reduction (Figure S2). The surface coverage of oxide at bare Au electrodes has been determined at $\Gamma_{AuO/Au(OH)} \sim 2.9 \times 10^{-11}$ mol cm^{-2}, whereas thiol coverage at modified electrodes has been measured to be $\Gamma_{thiol} \sim 2.2 \times 10^{-11}$ mol cm^{-2}. Thus, the ratio of thiol coverage can be roughly estimated at ∼75% of the area of our electrodes.

In addition to thise electrochemical evidence, the presence of Au oxide clusters is supported by SEM micrographs, which exhibit extensive occurrence of defects across mercaptopyridine layers (Supporting Information, Figure S3). The thiol coverage is not homogeneous, exhibiting roughness and cavities at micrometric level with sizes of a few hundreds of nanometers. Conceivably, smaller nonobservable defects are present in the mercaptopyridine layer, hidden by metal coating during sample preparation. Thus, the enhancing abilities exhibited by the FF-MNSs may be ascribed to preconcentration of urea species at peptide tapes, from which they diffuse down to surface where Au oxide clusters are available to behave as catalyst sites.

The cooperative effect leading to improvement on sensitivity may also be related to attractive interactions between urea and peptides either via cation−π bonds between benzene rings and charged *N*-termini or via strong H-bonds between carbonyl/amide units and urea N-groups. Similar to the proposed mechanism for urea hydrolysis at the active sites of urease,[45] the OH terminal at AuOH is positioned to provide an interaction through the carbonyl oxygen. This configuration leads to a tetrahedral intermediate that decomposes to release an NH_3 species and the possible formation of carbamic acid, followed by spontaneous decomposition into ammonia and carbon dioxide, which has a very short detection time (see Figure 6).[46]

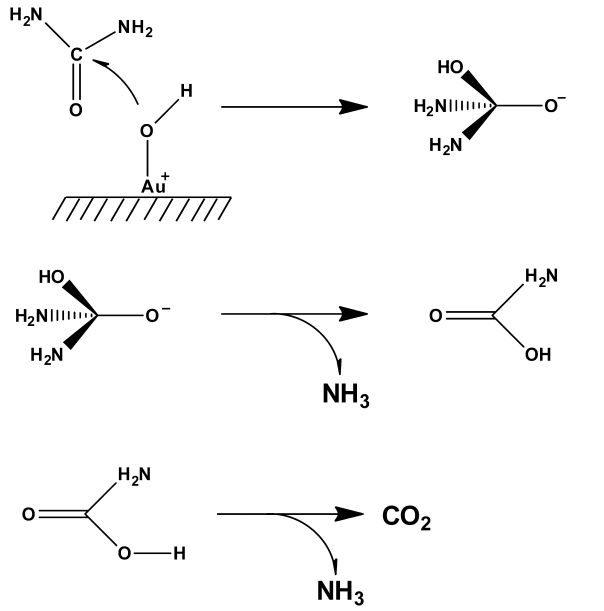

Figure 6. Proposed mechanism for urea hydrolysis at the electrodes described in this work. The OH terminal at AuOH provides an attack through the carbonyl oxygen, thereby generating a tetrahedral intermediate that decomposes into an NH_3 species. The reaction is followed by the possible formation of carbamic acid, which spontaneously decomposes into ammonia and carbon dioxide.

The reproducibility of our experimental results was verified using a standard urea concentration of 200 μmol L^{-1}. The FF-MNSs/MCP/Au electrodes exhibited a relative standard deviation of approximately 3.2% across three experimental trials. The stability of the electrode was measured over a period of 15 days, and the activity of the electrode was 90% if stored at 5 °C when not in use. No enzymes were employed; thus, long-term stability of the electrode was obtained. We also performed a recovery test by analyzing three parallel tap water samples that contained 60 mg mL^{-1} urea. This test was completed in 0.1 mol L^{-1} NaOH as a supporting electrolyte, and a recovery of 98% was observed.

dx.doi.org/10.1021/la502315m | *Langmuir* 2014, 30, 11464−11473

4. CONCLUSIONS

Here, we report a simple biosensor for the detection of ammonium and urea through a nonenzymatic route. The novelty of our approach is the use of a solid-vapor strategy to drive the crystalline structure of FF-MNS and lead to a distinct chemical behavior at interfaces between peptide and thiol. In this configuration, our method provides a unique architecture for gathering peptide micro/nanostructures (which are able to preconcentrate NH_4^+ species) and AuOH clusters to catalyze redox reactions. Unlike the tubular shape typically observed for FF-based assemblies prepared under similar conditions, our structures exhibit a clear tapelike morphology with thicknesses ranging from a few hundred nanometers to several micrometers. These characteristics are likely created by the mercaptopyridine substrate during the self-assembly. In addition, this shape likely has a positive effect because the flat surface of tapes can facilitate the buildup of analytes on electrodes.

For samples incubated under water vapor, the crystalline symmetry of our arrays can be described by the $P6_1$ space group, as previously reported for FF nanotubes.[13] However, the former structural model devised for solution-prepared assemblies did not account for all details of the XRD data raised in this work; thus, further refinements were necessary to interpret our diffraction patterns. These refinements changed the organization of water molecules within the assemblies to form long helixlike chains across the peptide matrix. We believe that this finding opens interesting possibilities for proton-conducting channels and ionic-transporter membranes. When samples were obtained under aniline vapor, the crystal structure was adequately described by an orthorhombic $P22_12_1$ space group. In addition, these orthorhombic-ordered structures were observed to be highly stable on the mercaptopyridine layer, in contrast to the water-incubated assemblies. This structural difference is the key to the success of our electrodes because it provides a peptide interface containing nitrogen/oxygen sites that can establish strong bonds either with pyridine units at the substrate or with ammonium ions and urea, leading to the concentration of these analytes, presumably via cation$-\pi$ interactions and/or H-bonds.

The response of our FF-MNSs/MCP/Au electrodes toward urea, based on detection of ammonium ions, has been found to be linear in the range from 0.1 to 1.0 mmol L^{-1}. Sensitivity and detection limit have been determined, respectively, at 81.3 μA mmol L^{-1} cm^{-2} and 0.06 mmol L^{-1} (S/N = 3). These findings reveal a highly-sensible sensor capable to detect urea even below physiological levels of 1−100 mmol L^{-1}, typically observed in urine and blood serum.[3] In this case, samples require dilution previous to analytical measurements, which is potentially advantageous because it allows for a finer control of sensing conditions. For example, by diluting sample to low concentration levels attainable by our biosensor, it is possible to accurately adjust the pH in solution and thus reduce the action of interfering species.[59] Moreover, despite that other systems have catalytic performance similar to those exhibited in the current work, we have presented here a proof of concept for detecting urea without using enzyme as a mediator. This remarkable feature reduces dramatically the cost of these architectures because short peptides are more attractive either from the point of view of synthesis or from the point of view of long-term stability (enzymes are very susceptible to denaturation). Such results show that the prepared nonenzymatic urea biosensors have suitable analytical characteristics.

■ ASSOCIATED CONTENT

Supporting Information

Overall aspect of FF-MSs/MCP/Au electrodes obtained under aniline vapor; cyclic voltammograms used to estimate the percentage of thiol coating in our electrodes; electron micrographs from bare Au electrode and from mercaptopyridine-modified electrode. This material is available free of charge via the Internet at http://pubs.acs.org.

■ AUTHOR INFORMATION

Corresponding Author

*E-mail: wendel.alves@ufabc.edu.br. Tel.: +55 11 4996 0193. Fax: +55 11 4996 3166.

Notes

The authors declare no competing financial interest.

■ ACKNOWLEDGMENTS

We gratefully acknowledge the financial support from the Brazilian agencies FAPESP (Grants 2013/12997-0, 2008/10537-3, 2011/05374-0, and 2013/12674-6) and CNPq (Grants 474871/2010-0 and 305186/2012-4). This work was also supported by the INCT in Bioanalytics (FAPESP Grant 08/57805-2 and CNPq Grant 573672/2008-3). We also thank the Brazilian Nanotechnology National Laboratory (LNNano) for access to their SEM facilities (proposals SEM-LV-13040, SEM-FEG-11235, and Inspect-13995).

■ REFERENCES

(1) Taylor, A. J.; Vadgama, P. Analytical reviews in clinical biochemistry: The estimation of urea. *Ann. Clin. Biochem.* **1992**, *29*, 245−264.

(2) Vanholder, R.; De Smet, R.; Glorieux, G.; Argiles, A.; Baurmeister, U.; Brunet, P.; Clark, W.; Cohen, G.; De Deyn, P. P.; Deppisch, R.; Descamps-Latscha, B.; Henle, T.; Jorres, A.; Lemke, H. D.; Massy, Z. A.; Passlick-Deetjen, J.; Rodriguez, M.; Stegmayr, B.; Stenvinkel, P.; Tetta, C.; Wanner, C.; Zidek, W. Review on uremic toxins: Classification, concentration, and interindividual variability. *Kidney Int.* **2003**, *63*, 1934−1943.

(3) Chen, J.-C.; Chou, J.-C.; Sun, T.-P.; Hsiung, S.-K. Portable urea biosensor based on the extended-gate field effect transistor. *Sens. Actuators, B* **2003**, *91*, 180−186.

(4) Vostiar, I.; Tkac, J.; Sturdik, E.; Gemeiner, P. Amperometric urea biosensor based on urease and electropolymerized toluidine blue dye as a pH-sensitive redox probe. *Bioelectrochemistry* **2002**, *56*, 113−115.

(5) Singh, M.; Verma, N.; Garg, A. K.; Redhu, N. Urea biosensors. *Sens. Actuators, B* **2008**, *134*, 345−351.

(6) Dhawan, G.; Sumana, G.; Malhotra, B. D. Recent developments in urea biosensors. *Biochem. Eng. J.* **2009**, *44*, 42−52.

(7) Patzer, Ii. J. F.; Yao, S. J.; Wolfson, S. K., Jr; Ruppel-Kerr, R. Urea oxidation kinetics via cyclic voltammetry: Application to regenerative hemodialysis. *Bioelectrochem. Bioenerg.* **1989**, *22*, 341−353.

(8) Petrii, O. A.; Vassina, S. Y. Adsorption of urea on platinum at low positive potentials: The time dependence and unexpectedly strong effect on the oxidation of uni-carbon particles. *J. Electroanal. Chem.* **1993**, *349*, 197−209.

(9) Kotnik, D.; Novič, M.; LaCourse, W. R.; Pihlar, B. Cathodic reactivation of the gold electrode in pulsed electrochemical detection of carbohydrates. *J. Electroanal. Chem.* **2011**, *663*, 30−35.

(10) Zelzer, M.; Ulijn, R. V. Next-generation peptide nanomaterials: Molecular networks, interfaces and supramolecular functionality. *Chem. Soc. Rev.* **2010**, *39*, 3351−3357.

(11) Reches, M.; Gazit, E. Casting metal nanowires within discrete self-assembled peptide nanotubes. *Science* **2003**, *300*, 625−627.
(12) Demirel, G.; Buyukserin, F. Surface-induced self-assembly of dipeptides onto nanotextured surfaces. *Langmuir* **2011**, *27*, 12533−12538.
(13) Gorbitz, C. H. The structure of nanotubes formed by diphenylalanine, the core recognition motif of Alzheimer's β-amyloid polypeptide. *Chem. Commun.* **2006**, *22*, 2332−2334.
(14) Silva, R. F.; Araújo, D. R.; Silva, E. R.; Ando, R. A.; Alves, W. A. l-Diphenylalanine microtubes as a potential drug-delivery system: Characterization, release kinetics, and cytotoxicity. *Langmuir* **2013**, *29*, 10205−10212.
(15) Souza, M. I.; Silva, E. R.; Jaques, Y. M.; Ferreira, F. F.; Fileti, E. E.; Alves, W. A. The role of water and structure on the generation of reactive oxygen species in peptide/hypericin complexes. *J. Pept. Sci.* **2014**, *20*, 554−562.
(16) Lee, J. S.; Yoon, I.; Kim, J.; Ihee, H.; Kim, B.; Park, C. B. Self-assembly of semiconducting photoluminescent peptide nanowires in the vapor phase. *Angew. Chem., Int. Ed. Engl.* **2011**, *50*, 1164−1167.
(17) Yemini, M.; Reches, M.; Rishpon, J.; Gazit, E. Novel electrochemical biosensing platform using self-assembled peptide nanotubes. *Nano Lett.* **2004**, *5*, 183−186.
(18) Yemini, M.; Reches, M.; Gazit, E.; Rishpon, J. Peptide nanotube-modified electrodes for enzyme−biosensor applications. *Anal. Chem.* **2005**, *77*, 5155−5159.
(19) Matos, I. O.; Alves, W. A. Electrochemical determination of dopamine based on self-assembled peptide nanostructure. *ACS Appl. Mater. Interfaces* **2011**, *3*, 4437−4443.
(20) Cipriano, T.; Takahashi, P.; De Lima, D.; Oliveira, V., Jr; Souza, J.; Martinho, H.; Alves, W. Spatial organization of peptide nanotubes for electrochemical devices. *J. Mater. Sci.* **2010**, *45*, 5101−5108.
(21) Späth, A.; König, B. Molecular recognition of organic ammonium ions in solution using synthetic receptors. *Beilstein J. Org. Chem.* **2010**, *6*, 32.
(22) Bühlmann, P.; Pretsch, E.; Bakker, E. Carrier-based ion-selective electrodes and bulk optodes. 2. Ionophores for potentiometric and optical sensors. *Chem. Rev.* **1998**, *98*, 1593−1688.
(23) Singh, Y.; Dolphin, G. T.; Razkin, J.; Dumy, P. Synthetic peptide templates for molecular recognition: recent advances and applications. *ChemBioChem* **2006**, *7*, 1298−1314.
(24) Ryu, J.; Park, C. B. High-temperature self-assembly of peptides into vertically well-aligned nanowires by aniline vapor. *Adv. Mater.* **2008**, *20*, 3754−3758.
(25) Amaral, H. R.; Kogikoski, S., Jr; Silva, E. R.; Souza, J. A.; Alves, W. A. Micro- and nano-sized peptidic assemblies prepared via solid-vapor approach: Morphological and spectroscopic aspects. *Mater. Chem. Phys.* **2012**, *137*, 638−636.
(26) Andrade-Filho, T.; Ferreira, F. F.; Alves, W. A.; Rocha, A. R. The effects of water molecules on the electronic and structural properties of peptide nanotubes. *Phys. Chem. Chem. Phys.* **2013**, *15*, 7555−7559.
(27) Wang, M. J.; Du, L. J.; Wu, X. L.; Xiong, S. J.; Chu, P. K. Charged diphenylalanine nanotubes and controlled hierarchical self-assembly. *ACS Nano* **2011**, *5*, 4448−4454.
(28) Smith, Q. A.; Gordon, M. S.; Slipchenko, L. V. Benzene−pyridine interactions predicted by the effective fragment potential method. *J. Phys. Chem. A* **2011**, *115*, 4598−4609.
(29) Pratt, L. R.; Pohorille, A. Hydrophobic effects and modeling of biophysical aqueous solution interfaces. *Chem. Rev.* **2002**, *102*, 2671−2691.
(30) Rietveld, H. M. Line profiles of neutron powder-diffraction peaks for structure refinement. *Acta Crystallogr.* **1967**, *22*, 151−152.
(31) Cheary, R. W.; Coelho, A. A. Axial divergence in a conventional X-ray powder diffractometer. II. Realization and evaluation in a fundamental-parameter profile fitting procedure. *J. Appl. Crystallogr.* **1998**, *31*, 862−868.
(32) Cheary, R. W.; Coelho, A. A fundamental parameters approach to X-ray line-profile fitting. *J. Appl. Crystallogr.* **1992**, *25*, 109−121.
(33) Jarvinen, M. Application of symmetrized harmonics expansion to correction of the preferred orientation effect. *J. Appl. Crystallogr.* **1993**, *26*, 525−531.
(34) Gorbitz, C. H. Microporous organic materials from hydrophobic dipeptides. *Chem.—Eur. J.* **2007**, *13*, 1022−31.
(35) Kim, J.; Han, T. H.; Kim, Y.-I.; Park, J. S.; Choi, J.; Churchill, D. C.; Kim, S. O.; Ihee, H. Role of water in directing diphenylalanine assembly into nanotubes and nanowires. *Adv. Mater.* **2010**, *22*, 583−587.
(36) Macrae, C. F.; Bruno, I. J.; Chisholm, J. A.; Edgington, P. R.; McCabe, P.; Pidcock, E.; Rodriguez-Monge, L.; Taylor, R.; van de Streek, J.; Wood, P. A. Mercury CSD 2.0. New features for the visualization and investigation of crystal structures. *J. Appl. Crystallogr.* **2008**, *41*, 466−470.
(37) Toby, B. H. R factors in Rietveld analysis: How good is good enough? *Powder Diffr.* **2006**, *21*, 67−70.
(38) Gdaniec, M.; Liberek, B. Structure of cyclo(-l-phenylalanyl-l-phenylalanyl-). *Acta Crystallogr., Sect. C: Cryst. Struct. Commun.* **1986**, *42*, 1343−1345.
(39) Görbitz, C. H. Nanotube formation by hydrophobic dipeptides. *Chem.—Eur. J.* **2001**, *7*, 5153−5159.
(40) Souza, M. I.; Jaques, Y. M.; Andrade, G. P.; Ribeiro, A. O.; Silva, E. R.; Fileti, E. E.; Avilla, E. S.; Pinheiro, M. V. B.; Krambrock, K.; Alves, W. A. Structural and photophysical properties of peptide micro/nanotubes functionalized with hypericin. *J. Phys. Chem. B* **2013**, *117*, 2605−2614.
(41) Declan Burke, L.; O'Mullane, A. P. Generation of active surface states of gold and the role of such states in electrocatalysis. *J. Solid State Electrochem* **2000**, *4*, 285−297.
(42) Oesch, U.; Janata, J. Electrochemical study of gold electrodes with anodic oxide films—I. Formation and reduction behaviour of anodic oxides on gold. *Electrochim. Acta* **1983**, *28*, 1237−1246.
(43) Hamm, U. W.; Kolb, D. M. On the stability of reconstructed Au(100) surfaces in the presence of organic molecules. *J. Electroanal. Chem.* **1992**, *332*, 339−347.
(44) Vidotti, M.; Silva, M. R.; Salvador, R. P.; Torresi, S. I. C.; Dall'Antonia, L. H. Electrocatalytic oxidation of urea by nano-structured nickel/cobalt hydroxide electrodes. *Electrochim. Acta* **2008**, *53*, 4030−4034.
(45) Carter, E. L.; Flugga, N.; Boer, J. L.; Mulrooney, S. B.; Hausinger, R. P. Interplay of metal ions and urease. *Metallomics* **2009**, *1*, 207−221.
(46) Zambelli, B.; Musiani, F.; Benini, S.; Ciurli, S. Chemistry of Ni^{2+} in urease: Sensing, trafficking, and catalysis. *Acc. Chem. Res.* **2011**, *44*, 520−530.
(47) Massafera, M. P.; Córdoba de Torresi, S. I. Evaluating the performance of polypyrrole nanowires on the electrochemical sensing of ammonia in solution. *J. Electroanal. Chem.* **2012**, *669*, 90−94.
(48) Luo, Y.-C.; Do, J.-S. Amperometric ammonium ion sensor based on polyaniline-poly(styrene sulfonate-*co*-maleic acid) composite conducting polymeric electrode. *Sens. Actuators, B* **2006**, *115*, 102−108.
(49) Strehlitz, B.; Gründig, B.; Kopinke, H. Sensor for amperometric determination of ammonia and ammonia-forming enzyme reactions. *Anal. Chim. Acta* **2000**, *403*, 11−23.
(50) Shen, C.-Y.; Huang, C.-P.; Huang, W.-T. Gas-detecting properties of surface acoustic wave ammonia sensors. *Sens. Actuators, B* **2004**, *101*, 1−7.
(51) Connolly, E. J.; Timmer, B.; Pham, H. T. M.; Groeneweg, J.; Sarro, P. M.; Olthuis, W.; French, P. J. A porous SiC ammonia sensor. *Sens. Actuators, B* **2005**, *109*, 44−46.
(52) Srivastava, R. K.; Srivastava, S.; Narayanan, T. N.; Mahlotra, B. D.; Vajtai, R.; Ajayan, P. M.; Srivastava, A. Functionalized Multilayered Graphene Platform for Urea Sensor. *ACS Nano* **2011**, *6*, 168−175.
(53) Solanki, P. R.; Kaushik, A.; Ansari, A. A.; Sumana, G.; Malhotra, B. Zinc oxide-chitosan nanobiocomposite for urea sensor. *Appl. Phys. Lett.* **2008**, *93*, 163903.
(54) Rajesh; Bisht, V.; Takashima, W.; Kaneto, K. An amperometric urea biosensor based on covalent immobilization of urease onto an

electrochemically prepared copolymer poly(*N*-3-aminopropyl pyrrole-*co*-pyrrole) film. *Biomaterials* **2005**, *26*, 3683−3690.
(55) Luo, Y.-C.; Do, J.-S. Urea biosensor based on PANi(urease)-Nafion/Au composite electrode. *Biosens. Bioelectron.* **2004**, *20*, 15−23.
(56) Xu, Z.; Chen, X.; Qu, X.; Jia, J.; Dong, S. Single-wall carbon nanotube-based voltammetric sensor and biosensor. *Biosens. Bioelectron.* **2004**, *20*, 579−584.
(57) Ahuja, T.; Kumar, D.; Singh, N.; Biradar, A. M.; Rajesh. Potentiometric urea biosensor based on multi-walled carbon nanotubes (MWCNTs)/silica composite material. *Mater. Sci. Eng., C* **2011**, *31*, 90−94.
(58) Massafera, M. P.; Torresi, S. I. C. Urea amperometric biosensors based on a multifunctional bipolymeric layer: Comparing enzyme immobilization methods. *Sens. Actuators, B* **2009**, *137*, 476−482.
(59) Kovacs, B.; Dombi, N. G.; Toth, K. Optical biosensor for urea with improved response time. *Biosens Bioelectron.* **2003**, *18*, 111−118.